Thermographic Detection of separated Flow

You may also be interested in:

Infrared Imaging: Application of thermal imaging in the diagnosis of inflammatory changes of nasal sinusitis
F Ring, A Jung and J uber

Infrared Imaging: Thermal imaging in the screening diagnosis of crural varices in adolescents
F Ring, A Jung and J uber

Infrared Imaging: A case study in the diagnosis of a grade III ankle sprain using a combination of medical images
F Ring, A Jung and J uber

Effects of natural and forced cooling on thethermographic patterns of tumours
Cecilia M Feasey, M Davison and W B James

Development and applications of laser spectroscopic techniques related to combustion diagnostics
Marcus Aldén

The digitization and analysis of thermographic images (in medicine)
J Shimmins, M D M Kay, W B James et al.

A water surface as a thermal reference object for thermography
J Lubbers and J Steketee

Electric current solves mazes
Simon Ayrinhac

Thermographic properties of Sm3+-doped GdVO4 phosphor
M G Nikoli, D J Jovanovi, V orevi et al.

# Thermographic Detection of separated Flow

**C. Dollinger[1], N. Balaresque[2], A. P. Schaffarczyk[3], A. Fischer[1]**

[1]  Bremen Institute for Metrology, Automation and Quality Science (BIMAQ),
    University of Bremen, Bremen, Germany
[2]  Deutsche WindGuard Engineering GmbH, Bremerhaven, Germany
[3]  Kiel University of Applied Sciences, Kiel, Germany

E-mail: c.dollinger@bimaq.de

**Abstract**. Thermographic wind tunnel measurements, both on a cylinder as well as on a 2D airfoil, were performed at various Reynolds numbers in order to evaluate the possibility of detecting and visualizing separated flow areas. A new approach by acquiring a series of thermographic images and applying a spatial-temporal statistical analysis allows improving both the resolution and the information content of the thermographic images. Separated flow regions become visible and laminar/turbulent transitions can be detected more accurately. The knowledge about possibly present stall cells can be used to confirm two-dimensional flow conditions and support the development of more effective and silent rotorblades.

## 1.  Introduction and work objectives

Flow separation on a wind turbine's rotorblade, both as a stable or as a transient phenomenon, is not an uncommon sight on today's wind turbines. Flow separation does not only negatively affect performance and often increase unsteady loads, but can also be the cause of increased acoustic emissions. Although the determination of the location of the separated flow region for wind turbines in operation is currently possible using markers or sensors installed on the blade, this is a time consuming and costly operation. Current methods usually involve tufts, stall flags, or oil flow-visualization [1]. The precise positioning of these markers requires expertise, a working platform, and appropriate low-wind weather conditions to perform the installation. Due to the influence of tufts and oil on the immediate boundary layer, the location of the laminar/turbulent flow transition is affected.

Based on passive thermography measurements, a method has been developed to allow flow separation detection in a non-invasive way, which requires no preparation of the model. The method has proved to work with airfoils and cylinders in a wind tunnel, and is currently being tested on megawatt-class wind turbines in operation. There had been investigations regarding a thermographic detection of separated flow regions on airfoils in the past, but the results were provided with a actively heated model [2]. With respect to the small temperature differences between the different flow regions on a unheated rotorblade in operation, an image processing algorithm has been developed to enhance the contrast and enable a distinction of the regions with separated flow.

The paper shows thermographic results compared to surface pressure measurements and oil flow visualization in a wind tunnel. The results can be seen as a first proof-of-concept step towards passive flow separation detection on wind turbines in operation.

## 2. Approach and methods

### 2.1. Background
This work is based on the principles of the thermographic flow visualization [3]. This measuring method is directed to the measurement and evaluation of the flow conditions and ranges on an airfoil's surface. As there is no absolute agreement regarding the classification of flow ranges on a cylinder (4), in this case, the naming corresponds to the following order in ascending Reynolds number:

- Subcritical ($Cd \approx 1.2$),
- Critical ($Cd \approx [<1.2 : >0.2]$,
- Supercritical $Cd \approx [0.2 : 0.5]$,
- Transcritical.

During the critical regime, the drag coefficient decreases from ≈1.2 to 0.2. Whereas the decrease from 1.2 to 1.0 is subtle, the decrease from 1.0 to 0.2 can be very abrupt. The Cd range [1.0 : 0.2] is particularly unstable, and includes a flow state in which a one-sided separation bubble causes lift.

The flow condition mentioned in this paper corresponds to the early-critical regime, before the abrupt drag decrease takes place.

The surface temperature on an airfoil is influenced by a variety of parameters and can be correlated to the boundary layer flow conditions. The flow visualization is based on the heat exchange by convection, conduction and radiation between the airfoil and the surrounding flow. When the flow temperature is higher than the model, as in this wind tunnel case, because of the enhanced exchange of energy between flow and airfoil in the region of turbulent flow, an increase of the surface temperature compared to the region with laminar flow can be detected by a thermographic measuring system [5]. Subsequent image processing algorithms are capable to identify and locate the laminar/turbulent transition [6]. Figure 1 shows a processed thermographic image of a NACA 63618 airfoil in the wind tunnel. An image processing algorithm permits the detection of the transition by the evaluation of the local temperature differences.
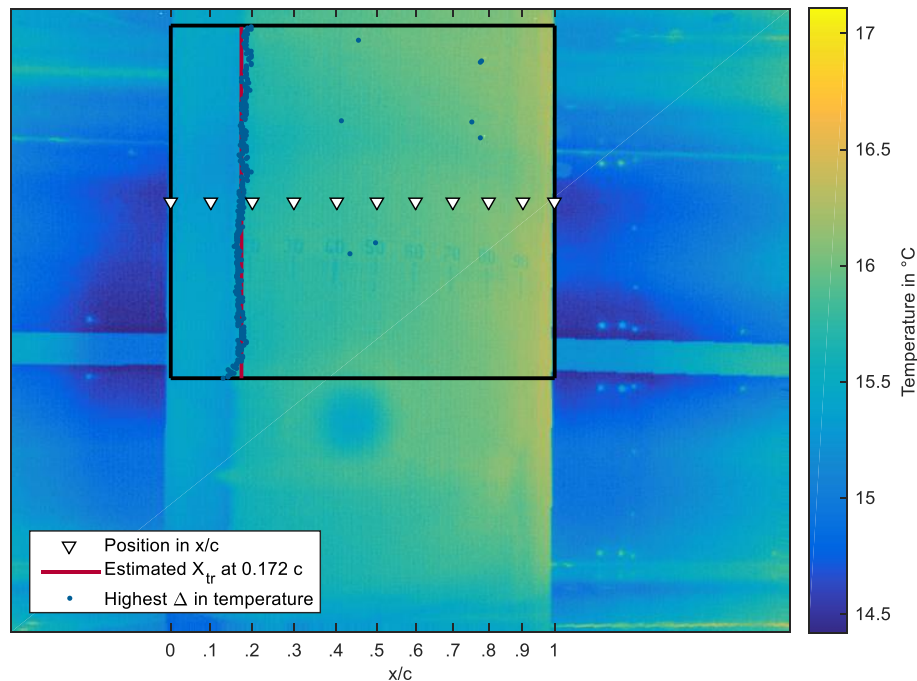


**Figure 1.** Example of the thermographic flow visualization on a NACA 63618 airfoil and the automated detection of the laminar/turbulent transition.

The results are generated and displayed by the Transition Finder software, which was developed by BIMAQ and Deutsche WindGuard Engineering GmbH. The highest temperature gradients (blue dots) within a region of interest are identified and the location of the transition is estimated by a probability density function (red line).The knowledge about the position of the laminar/turbulent transition and the location of the separated flow region can be used to design more effective aerodynamic profiles to reduce acoustic emissions and increase the energy yield [5]. On field measurements of wind turbines in operation, the rotorblades are heated by the sun and are cooled by the oncoming wind, causing the surface temperature of the turbulent region to be lower. The surface temperature difference in the wind tunnel, for the wind speed range presented here, is in the same order of magnitude as many on-site measurements performed by the authors, permitting proof of concept tests in the wind tunnel.

*2.2. Simulation*
It is well known that the flow around a cylinder consists of complex vortical structures [8] especially in the so called trans-critical region, were the drag coefficient drops considerably from about 1 to less than 0.4. Apparently an interplay between laminar separation, transition, turbulent re-attachment and turbulent separation further downstream may be observed [9]. A very striking feature is that in early critical flow region (Re 3.4E5) separation occurs at an angle of about 70° but at trans-critical conditions (Re 3.8E5) much later at about 140°. Concerning CFD, up to now only LES [10] with extremely fine 3D meshes and corresponding small time steps seem to model this type of flow accurately. RANS, URANS and hybrid models (a mixture of URANS and LES models) [11] therefore may not be appropriate, hence an experimental setup with oil flow visualization was chosen for the preliminary comparisons shown in this paper.

*2.3. Measurement set-up*
First tests were conducted at the Deutsche WindGuard aero-acoustic wind tunnel in Bremerhaven, a closed-return type tunnel in which laminar flows (Tu < 0.3 %) at speeds of up to 100 m/s and chord-Reynolds numbers of up to 6E6 can be achieved. In addition to the flow tests in the wind tunnel, measurements at an operating wind turbine were performed. Extensive measurements on several 800 mm chord 2D airfoils and cylinders were performed, in order to make use of the different flow regimes to demonstrate the method. Pressure integration and force balances above and below the turntables were used to measure lift and drag. The presented measurements were performed at up to 55 m/s, reaching Re 3.0E6 for the stalled airfoil, and 5.2E5 for the cylinder[1]. The thermographic measurements were accomplished with a cooled InSb-focal-plane-array with a resolution of 640 x 512 pixels. It is sensitive between 2 and 5 µm and works with a thermal resolution better than 25 µK. It observes the test section through a $CaF_2$-window.

*2.4. Statistical approach*
In earlier approaches using thermography on unheated specimens, only regions with laminar or turbulent flow could be distinguished [3,4,12]. This can be explained by the limited information that a single thermal image, taken with small temperature differences on the specimen, contains. Due to the unsteady conditions in regions of flow separation, there is a chance to observe small temperature changes in a time-series of thermographic images. Therefore, an image processing algorithm based on a spatial decomposition, statistical evaluation and reconstruction of the thermographic image-series [7] was implemented.

The spatial-temporal analyses and the statistical evaluation of the modified image-series enable the visualization of regions with separated flow. It can be distinguished between regions with a high and a low "Temperature Fluctuation Index (TFI, standard deviation of the reconstructed data).

---

[1] The airfoil was tested up to 95 m/s (Re 5E6) and the cylinder up to 65 m/s (Re 6E5).

## 3. Statistical analysis of time-variant thermographic data

### 3.1. Measurements on a cylinder

Measurements of a cylinder spanning the test section were performed in the Deutsche WindGuard aero-acoustical wind tunnel in Bremerhaven. To evaluate and compare the thermographic measuring data, oil flow visualization images were taken and surface pressure measurements were conducted.

### 3.1.1. Experimental setup and model

The mounting-setup and a design-drawing are shown in figure 2. The cylinder with 73 pressure taps and 1 flush-mounted microphone was manufactured out of POM (polyoxymethylene). The material of choice allows a high quality machining and, due to its thermal properties, is appropriate for thermal imaging without the need of an additional surface preparation, such as when using metallic models.
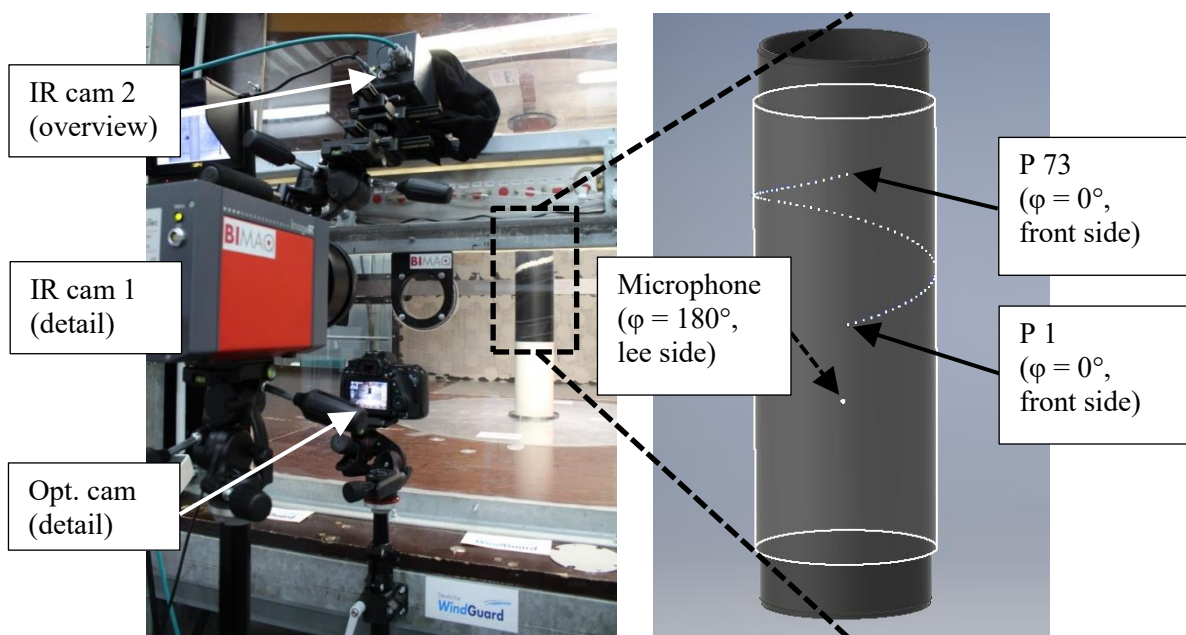


**Figure 2.** Cylinder mounted in the closed test section of the WindGuard aero-acoustic wind tunnel (left). Mid-section of the cylinder indicating the location of the pressure taps (right).

The model consists of 3 parts: The center part, in which the pressure taps and the microphone are located, was manufactured of black POM, whereas the uninstrumented lower and upper sections were manufactured of white POM to provide more flexibility toward flow visualization techniques and pigment choice. The cylinder was assembled outside the test section and mounted in one piece between two turntables for testing purposes. No external heating was used during the measurements.

### 3.1.2. Surface pressure measurements

The 73 pressure taps have an inner diameter of d = 0.3 mm, are equally spaced (5° steps in azimuthal direction) and the middle line is inclined by 15° to avoid disturbances between pressure taps. The tests showed that none of the pressure taps cause a premature laminar-turbulent transition and that all are in working order. The two pressure taps located at $\varphi = 0$ depicted in figure 2 are roughly 135 mm apart from each other. The microphone is intended for a future acoustic analysis of vortex shedding, with rotation of the cylinder. During this test the Cylinder was not rotated.

The results of the surface pressure measurements at two different Reynolds numbers can be found in figure 3. The results are overlaid on data from literature [9]. $S_L$ and $S_T$ mark the regions of laminar and turbulent separation. $S_L$ is often identifiably by a kink in the pressure distribution, whereas $S_T$ marks the region in which the base pressure level is reached (no more pressure recovery takes place).
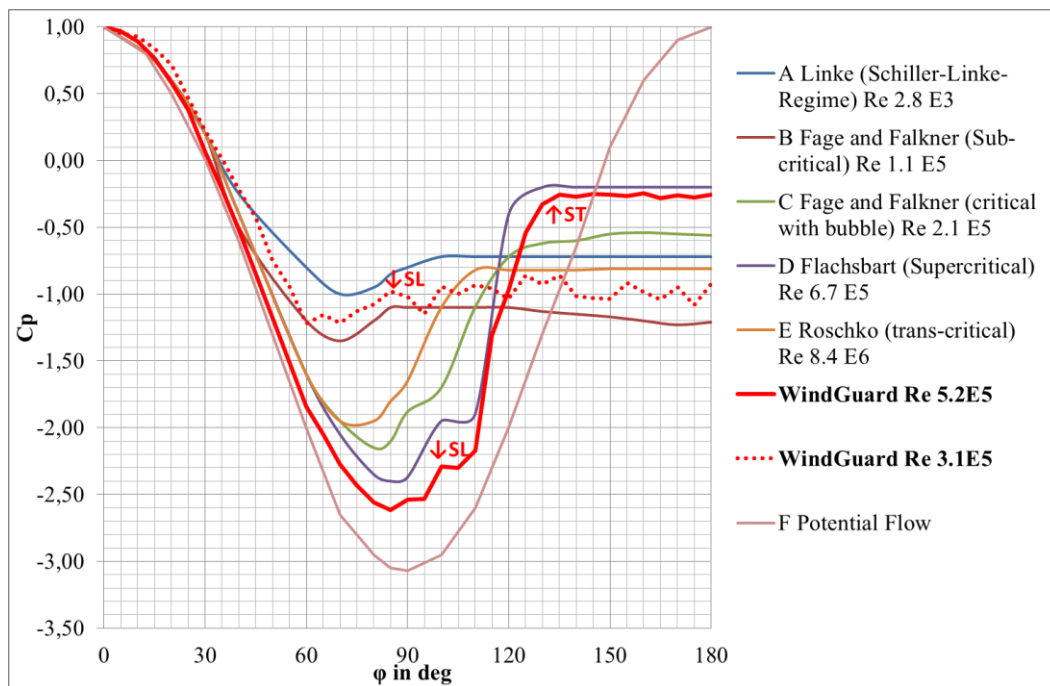
**Figure 3**. Pressure measurements at two Reynolds numbers overlaid on data which can be found in [9].

Pressure measurements were performed simultaneously to all measurements, using independent connected high range piezo pressure sensors for each port. The large scatter observed in the separated flow region for the Re 3.1E5 run is due partly to the high range pressure sensors used and to a limited averaging time during the measurement of a highly dynamic region flow. The connecting tubes are of small diameter and the pressure sensors are located far away, causing a strong low-pass pressure filtering.

*3.1.3. Thermographic measurements and oil flow visualization*
The following figures (figure 4 and figure 5) show the thermographic data compared to the oil flow visualization of two different states of the flow at the cylinder. Figure 4 shows the images at a Re 3.1E5 (critical) and figure 5 shows the cylinder at Re 5.2E5 (super critical).

The upper image in each figure corresponds to the original, unprocessed images as delivered by the thermographic measuring system (temperatures in these images are normalized with the mean temperature ($t_{ave}$). The lower image shows the processed images whereas the middle image shows oil-visualization in direct comparison. The processed images were computed by the spatial-temporal combination of 30 periodic temporally-equidistant thermographic frames. The resulting "Temperature Fluctuation Index" (TFI) indicates how strong the changes in temperature are within the temporal sample. In all of the images the positions are marked chordwise in x/c and in degrees. The unsymmetrical distribution of the markers is due to the displaced angle of view of the cameras. The processed images show additional regions within the separated flow region that will not be further addressed at the moment.

A daylight fluorescent pigment was used together with silicone oil for flow visualization. The images were acquired with the wind tunnel in operation. Due to the fact that the separation location is extremely sensitive to surface roughness and geometrical steps, care was taken to use as little oil-pigment solution as possible. As soon as the oil layer gets thicker and accumulation occurs (i.e. in a laminar separation bubble) the separation point can shift noticeably.

A series of optical images were taken every 30 seconds in order to document the settling of the flow lines. This permits waiting long enough to achieve an appropriate image before local

accumulation artificially modifies the flow field. Figure 4 shows the cylinder at a critical Re of Re 3.1E5 with a drag coefficient near 1.
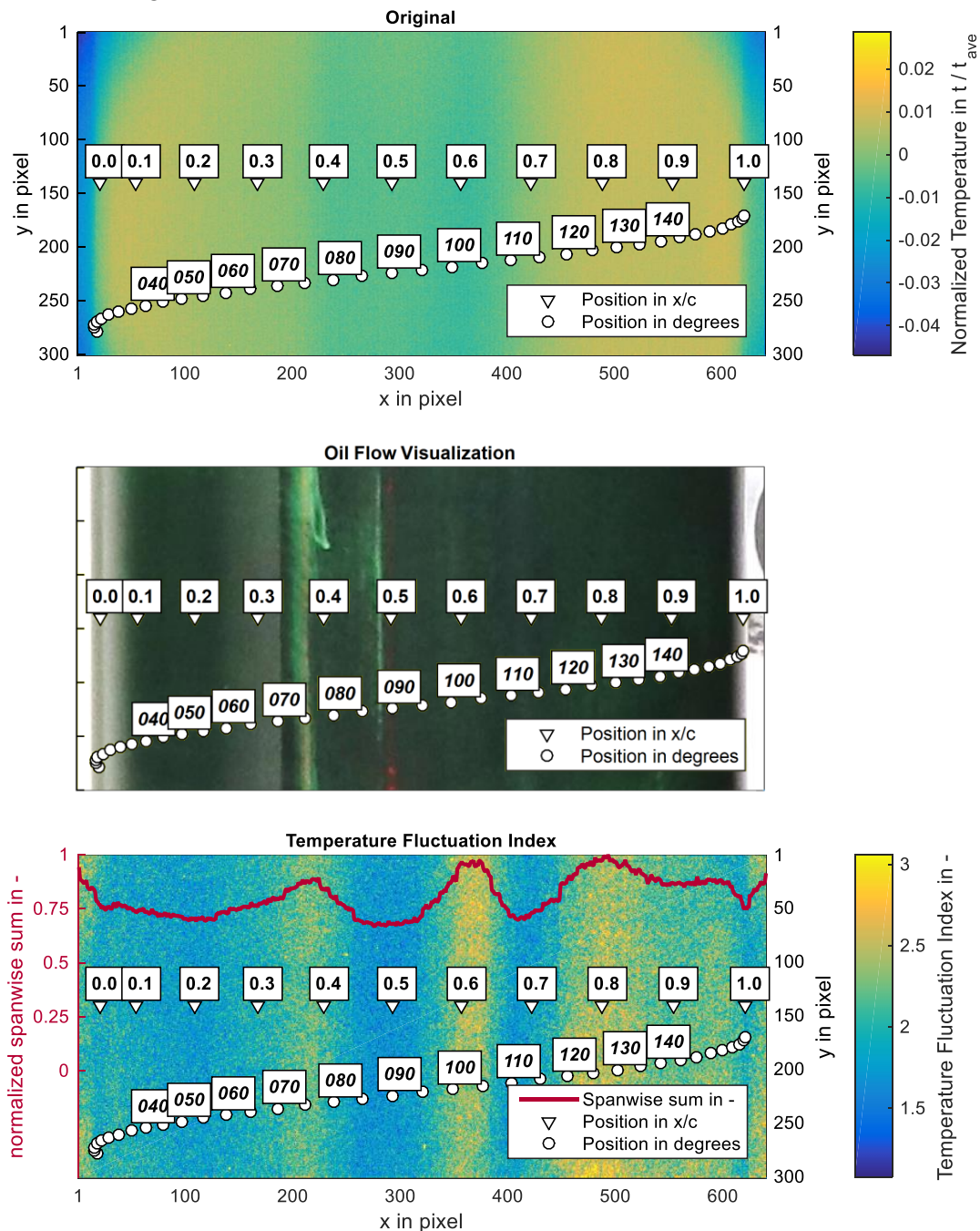


**Figure 4.** Cylinder at Re 3.1E5, $C_D \approx 1$, critical Re. Comparison of an unprocessed thermographic image to a picture of oil-pigment flow visualization and to a processed thermographic image.

Even though the flow pattern is not evident (extremely little oil was used to affect the flow as little as possible), one explanation would correspond to separation through a short laminar separation bubble, with separation occurring at 88° in the oil flow visualization. The 90° region shows a very low TFI what would correlate to a separation line that does not move in time with low flow speed fluctuations. Both the 76° and 103° show a high TFI. The 114°±5 region is stable, and as from 120° onwards is

again highly dynamic. The red vertical line at 90° corresponds to a line-laser positioned over the 90° pressure tap as a reference. The second laser that can be seen at 75° was used as an aid to indicate certain positions during the measurement.

In figure 5, the resulting images of the cylinder at a super critical Re of Re 5.2E5 with a drag coefficient of 0.4 are shown.
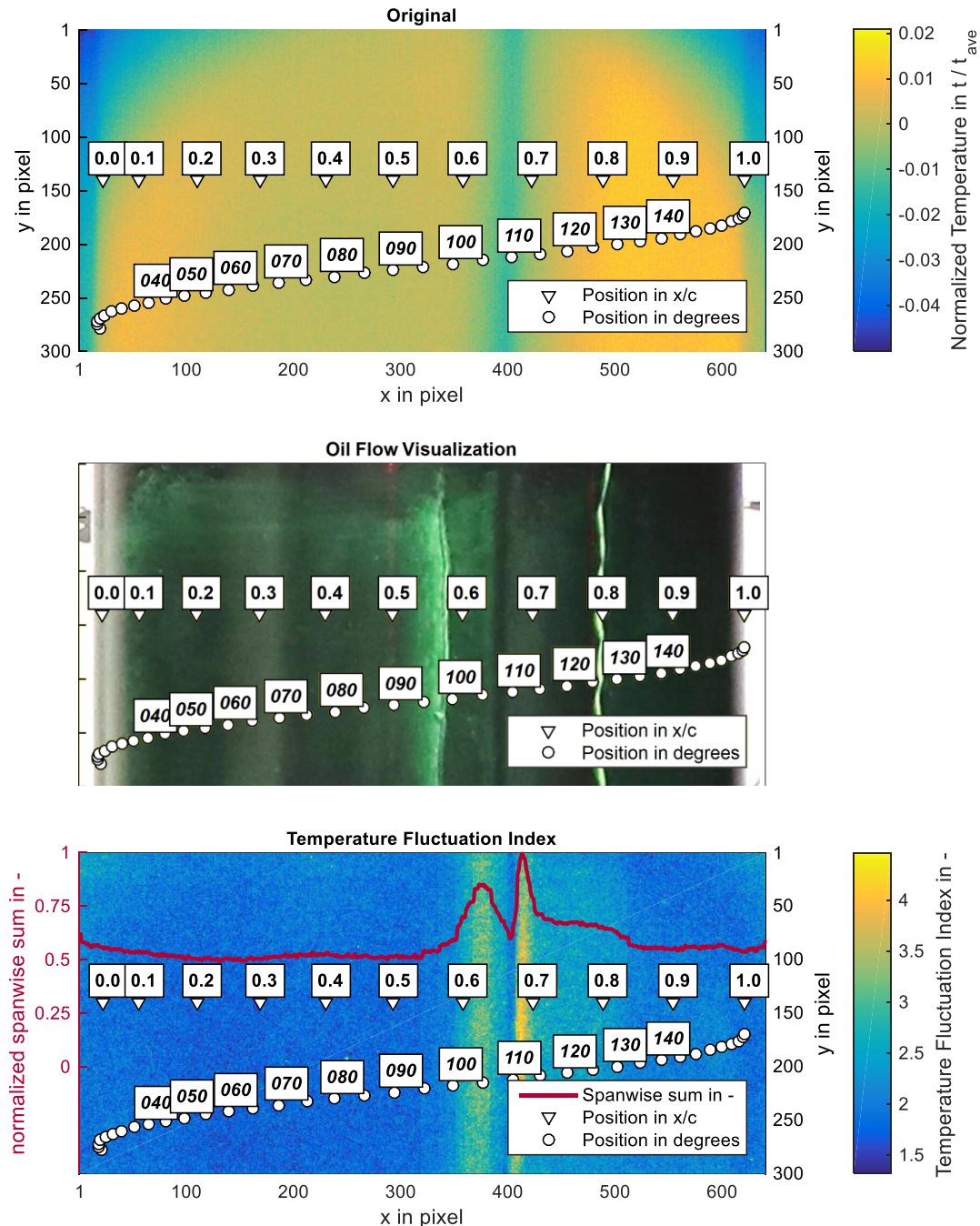


**Figure 5.** Cylinder at Re 5.2E5, $C_D \approx 0.3$, super critical Re. Comparison of an unprocessed thermographic image to a picture of oil-pigment flow visualization and to a processed thermographic image.

The observed pattern in flow direction approximately corresponds to a laminar separation at 99° in flow visualization and at 101° in thermal imaging. A reattachment at 108° in flow visualization and at

111° in thermal imaging followed by a turbulent separation at 127° in flow visualization and at 132° in thermal imaging can be observed. An inspection of the flow pattern after the wind tunnel was stopped showed that the region after 132° corresponds to a reverse flow region. The oil flow visualization has an effect on the flow and causes the transition and separation lines to move forward (left) due to the increase in surface roughness.

A second thermographic camera provided overview images in addition to the detailed processed images. These images are shown in figure 6 and are meant to evaluate the overall spanwise flow. A slight deviation from a pure 2D flow can be observed in figure 6 at the joint between two of the model parts for the right image (y ≈ 150 pixels). The increased roughness of the joint, even though it was filled and sanded, affects the flow and moves the separation position forward.
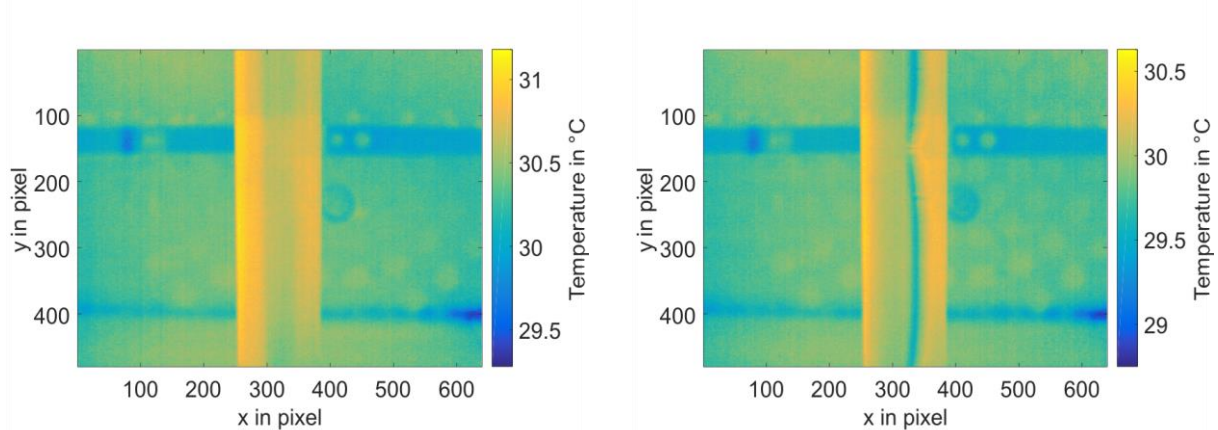


**Figure 6.** Overview images of the two states. Cylinder at early critical Re (Cd ≈ 1) on the left and at super critical Re (Cd ≈ 0.3) on the right thermographic image.

### 3.2. Measurements on an airfoil model with a thickness of 38%

In addition to the measurements on the cylindrical model, measurements on airfoil models, as they are used to measure the aerodynamic performance of wind turbine blades, were performed. The following paragraphs show the setup and the results on one of these airfoils. The image processing algorithm works similar on other airfoils at high angles of attack with comparable results.

### 3.2.1. Experimental setup and model

For reasons of clarity a relatively thick (38%) airfoil with a chord-length of 800 mm, belonging to the root section of a LM rotorblade with a length of 37 m, is chosen. The airfoil is shown in deep stall at an angle of attack of 24 degrees. As it is a model made of balsa wood and aluminum, the surface is coated with two layers of PVC-film to enhance the contrast between the different flow regions.

### 3.2.2. Thermographic measurements

When using local measurement methods such as airfoil surface pressure integration to calculate an airfoil's characteristics (lift, drag and moment), it is important to assess the extent of 2D flow conditions. An example for the measurement of airfoil models can be found in figure 7. With the image processing, the region with separated flow, as well 3D wall effects on both upper and lower turntable become (more) visible. As in the figures above, flow is from left to right and original and processed images are compared.
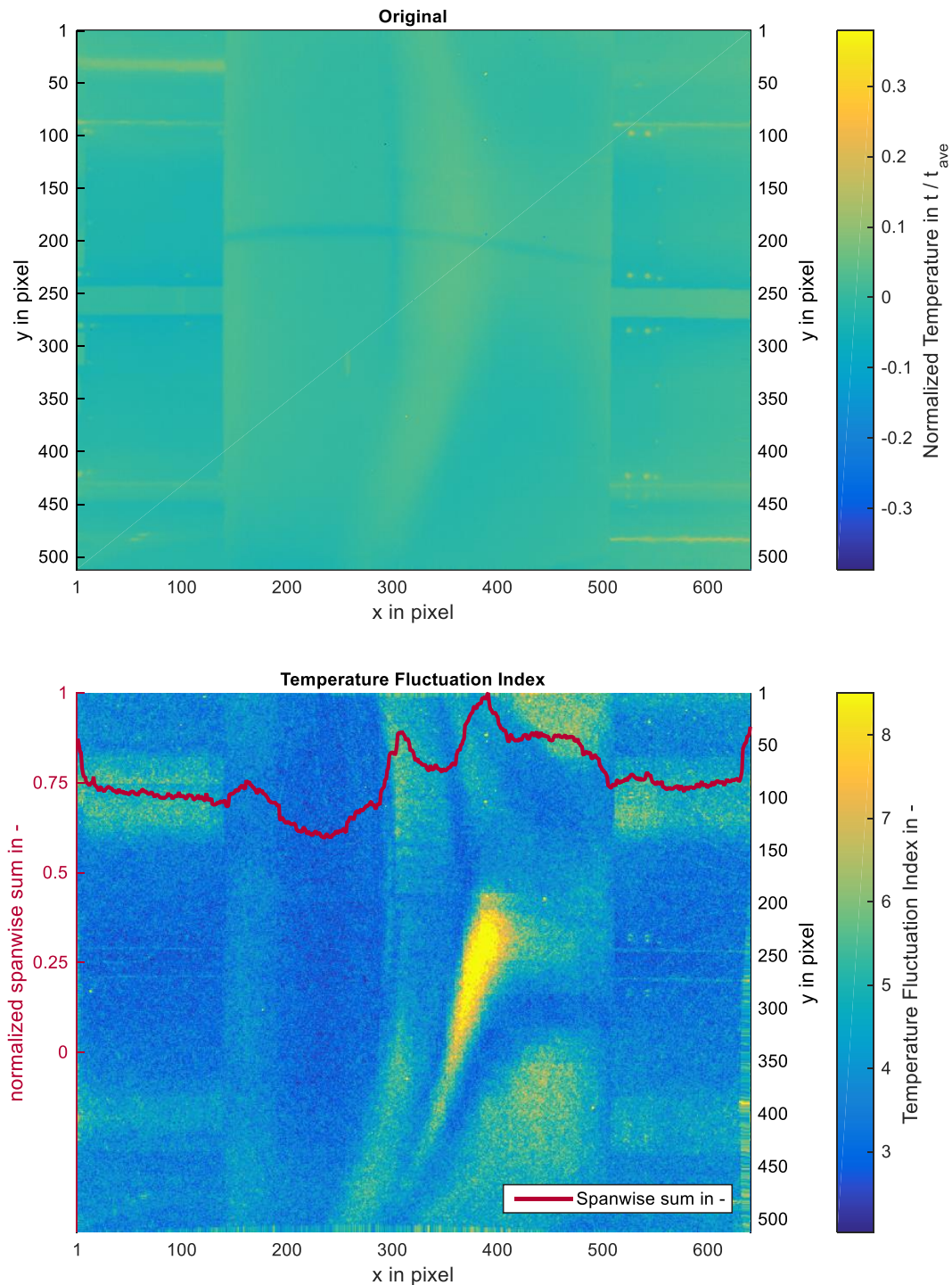
**Figure 7.** Airfoil at Re 3.0E6. The stalled airfoil with a thickness of 38% and a chord-length of 800 mm is positioned at an angle of attack of 24 degrees.

## 4. Conclusions

A method has been developed in which the post-processing of several thermographic images goes beyond displaying the laminar/turbulent transition on a non-heated airfoil. Areas that are characterized by differences in their transient flow regimes, such as separated flow regions, are revealed. This is

both useful in wind tunnels to evaluate stall and the extent of 2D flow conditions, and on the field to assess the real operating conditions of wind turbines in operation. The information obtained can help identify problem zones, and will be useful when deciding where to place flow control add-ons. The method was successfully compared to traditional surface pressure measurements and oil-flow visualization methods in a wind tunnel. In contrast to the established methods the new approach enables a very fast and absolutely noninvasive way to visualize separated flow in wind tunnel tests. Next steps will include measurements on standstill and running wind turbines to estimate the possibility to transfer the method to on-site measurements. For the processing it is required to compare images in which the observed object is in exactly the same location in every image. In order to analyze future field measurements, as opposed to wind tunnel tests, a preliminarily alignment of the images is required. This alignment can performed by the enhanced correlation coefficient maximization presented in [13]. To enable an alignment with similar images, an optical trigger device, which is able to take a picture every rotation of the rotor, was developed and used for first tests on site.

## 5. Acknowledgement

## References

[1]   Vey S et al: *Extracting quantitative data from tuft flow visualizations on utility scale wind turbines*. Journal of Physics: Conference Series 524, 2014.

[2]   Montelpare S and Ricci R: A thermographic method to evaluate the local boundary layer separation phenomena on aerodynamic bodies operating at low Reynolds number. International Journal of Thermal Sciences 43 (2004), 315-329.

[3]   Bæk P and Fuglsang P: *Experimental Detection of Transition on Wind Turbine Airfoils*. Proceedings of EWEC European Wind Energy Conference 2009.

[4]   Chen S-S: *Flow-induced vibration of circular cylindrical structures*. Vol. 414. Washington, DC: Hemisphere publishing corporation, 1987.

[5]   Dollinger C et al: *Aeroacoustic Optimization of Wind Turbine Airfoils by Combining Thermographic and Acoustic Measurement Data*. DEWI Magazine No. 43, 2013.

[6]   Crawford B K et al: *Quantitative Boundary-Layer Transition Measurements Using IR Thermography*. AIAA SciTech, 13-17, 2014.

[7]   Wu H Y et al: *Eulerian Video Magnification for Revealing Subtle Changes in the World*. ACM Transactions on Graphics, Volume 31, Number 4 (Proc. SIGGRAPH), 2012

[8]   Williamson C H K: *Vortex Dynamics in the Cylinder Wake*. Annual Rev. Fluid Mechanics (1996) 28:477-539

[9]   Gölling B: *Experimentelle Untersuchungen des laminar-turbulenten Überganges der Zylindergrenzschichtströmung Zylindergrenzschichtumströmung* (in German), Dissertation (PhD thesis). http://hdl.handle.net/11858/00-1735-0000-0006-B5AF-5, 2001

[10]  Rodríguez I et al: *High performance computing of the flow past a circular cylinder at critical and supercritical Reynolds numbers*. Procedia Engineering 61 (2013), 166-172

[11]  Soerensen N N: *3D CFD computations of transitional flows using DES and correlation based transition model*. Risoe-R-1692(EN), July 2009

[12]  Dollinger C et al: *Thermographic Measurement Method For Turbulence Boundary Layer Analysis On Wind Turbine Airfoils*. AWEA WINDPOWER 2014 Conference and Exhibition. AWEA American Wind Energy Association, Las Vegas, 2014.

[13]  Evangelidis G D and Psarakis E Z: *Parametric image alignment using enhanced correlation coefficient maximization*. Pattern Analysis and Machine Intelligence, IEEE Transactions on, 30(10), 1858-1865, 2008.